Table 1. *Gradients of planarity criteria calculated for the model structure*

Gradients are normalized under $|\nabla F_{A,z}| = 10\,000$. Here *A*, *B*, *C* are different atomic types (Fig. 2).

| | | *A* | | | *B* | | | *C* | | |
|---|---|---|---|---|---|---|---|---|---|---|
| $\Delta r$ | Criterion | $\nabla_x$ | $\nabla_y$ | $\nabla_z$ | $\nabla_x$ | $\nabla_y$ | $\nabla_z$ | $\nabla_x$ | $\nabla_y$ | $\nabla_z$ |
| 0·10 | $f_V$* | −484 | 0 | 10 000 | −242 | 0 | −10 000 | −121 | 775 | 0 |
| 0·25 | $f_V$ | −1210 | 0 | 10 000 | −605 | 0 | −10 000 | −303 | 1 938 | 0 |
| 0·50 | $f_V$ | −2424 | 0 | 10 000 | −1212 | 0 | −10 000 | −606 | 3 876 | 0 |
| 0·75 | $f_V$ | −3630 | 0 | 10 000 | −1815 | 0 | −10 000 | −909 | 5 813 | 0 |
| 1·00 | $f_V$ | −4848 | 0 | 10 000 | −2424 | 0 | −10 000 | −1212 | 7 752 | 0 |
| 1·25 | $f_V$ | −6060 | 0 | 10 000 | −3030 | 0 | −10 000 | −1515 | 9 690 | 0 |
| 1·50 | $f_V$ | −7260 | 0 | 10 000 | −3630 | 0 | −10 000 | −1815 | 11 625 | 0 |
| 0·10–1·25 | $f$† | 0 | 0 | 10 000 | 0 | 0 | −10 000 | 0 | 0 | 0 |
| 1·50 | $f$‡ | 0 | 0 | 0 | 0 | 0 | 0 | 0 | 10 000 | 0 |

* $f_V = \lambda_1\lambda_2\lambda_3$ [see (10), (15)].
† $f = \lambda_1$ [see (14)]
‡ Here normalization is under the condition $|\nabla f_{C,z}| = 10\,000$.

important property of an analytical expression in terms of atomic parameters. The exact gradient can also be easily calculated, which makes it possible to refine optimal plane parameters. This method of calculation of this criterion and its gradient may be included in any refinement program.

The author thanks O. M. Liguinchenko for help with the English and the referees for essential improvements in the text.

### References


CHAMBERS, J. L. & STROUD, R. M. (1977). *Acta Cryst.* B**33**, 1824–1837.

DODSON, E. J., ISAACS, N. W. & ROLLETT, J. S. (1976). *Acta Cryst.* A**32**, 311–315.

FRAZER, R. A., DUNCAN, W. J. & COLLAR, A. R. (1938). *Elementary Matrices and Some Applications to Dynamics and Differential Equations.* Cambridge Univ. Press.

FRENCH, S. (1975). *The Interpretation of X-ray Crystallographic Data on Proteins.* DPhil thesis, Univ. of Oxford, England.

HANEEF, I., MOSS, D. S., STANFORD, M. J. & BORKAKOTI, N. (1985). *Acta Cryst.* A**41**, 426–433.

HENDRICKSON, W. A. & KONNERT, J. H. (1980). In *Biomolecular Structure, Function, Conformation and Evolution*, edited by R. SRINIVASAN, Vol. 1, pp. 43–57. Oxford: Pergamon Press.

HERMANS, J. JR & MCQUEEN, J. E. JR (1974). *Acta Cryst.* A**30**, 730–739.

KIM, K. V., NESTEROV, YU. E. & CHERKASSKIY, B. V. (1984). *Dokl. Akad. Nauk SSSR*, **275**, 1306–1309.

KORN, G. A. & KORN, T. M. (1968). *Mathematical Handbook for Scientists and Engineers.* New York: McGraw-Hill.

LEVITT, M. & LIFSON, S. (1969). *J. Mol. Biol.* **46**, 269–279.

LUNIN, V. YU. & URZHUMTSEV, A. G. (1985). *Acta Cryst.* A**41**, 327–333.

SCHOMAKER, V., WASER, J., MARSH, R. & BERGMAN, G. (1959). *Acta Cryst.* **12**, 600–604.

TEN EYCK, L. F., WEAVER, L. H. & MATTHEWS, B. W. (1976). *Acta Cryst.* A**32**, 349–350.

TOMLIN, L. J. (1987). *J. Appl. Cryst.* **20**, 48–53.

URZHUMTSEV, A. G., LUNIN, V. YU. & VERNOSLOVA, E. A. (1989). *J. Appl. Cryst.* **22**, 500–506.

WASER, J. (1963). *Acta Cryst.* **16**, 1091–1094.


*Acta Cryst.* (1991). A**47**, 727–735

# Diffraction Streaks from the Chimney Ladder Structure in an $(Sr_{1.5}Ca_{1.5})Cu_{5+\delta}O_y$ Crystal

BY XIAO-JING WU, EIJI TAKAYAMA-MUROMACHI, SHIGERU SUEHARA AND SHIGEO HORIUCHI

*National Institute for Research in Inorganic Materials, Tsukuba, Ibaraki*, 305, *Japan*

(*Received* 17 *January* 1991; *accepted* 4 *June* 1991)


## Abstract

A crystal of $(Sr_{1.5}Ca_{1.5})Cu_{5+\delta}O_y$ has been studied by means of electron diffraction analysis and high-resolution transmission electron microscopy. A chimney ladder structure has been identified in the crystal, which is composed of two sets of incommensurate orthorhombic sublattices $L_1$ and $L_2$ with $a = a_1 = a_2 = 1{\cdot}28$, $b = b_1 = b_2 = 1{\cdot}13$, $c_1 = 0{\cdot}390$ and $c_2 = 0{\cdot}275$ nm. Diffraction streaks have been observed in electron diffraction patterns, *i.e.* there is a set of reflection planes parallel to $\mathbf{a}^*\mathbf{b}^*$ related to $L_2$. A structure model with initial phase disorder has been proposed to explain such diffraction streaks. A mathematical


0108-7673/91/060727-09$03.00

inference as well as an optical diffraction method have confirmed this model. Observed high-resolution images together with calculated ones gave a direct verification for the initial phase disorder.

## 1. Introduction

$(Sr_{1.5}Ca_{1.5})Cu_{5+\delta}O_y$ is an impurity phase which often coexists with Bi-based superconductors (Horiuchi, Shoda, Wu, Nozaki & Tsutsumi, 1990). The electron diffraction analysis shows that the crystal is composed of two sets of orthorhombic sublattices, which are incommensurate along the $c$ axis with $a = 1{\cdot}28$, $b = 1{\cdot}13$, $c_1 = 0{\cdot}390$ and $c_2 = 0{\cdot}275$ nm. In other words, the crystal has a so-called chimney ladder structure (Wu & Horiuchi, 1991).

Similar crystals have been studied by X-ray single-crystal diffraction. Kato, Takayama-Muromachi, Kosuda & Uchida (1988) have studied $M_{10}Cu_{17}O_{29}$ ($M$ = Bi, Sr, Ca), McCarron, Subramanian, Calabrese & Harlow (1988) have studied $(Sr_{14+x}Ca_x)Cu_{24}O_{41}$ ($x = 0$–$8$) and Siegrist, Schneemeyer, Sunshine, Waszczak & Roth (1988) have studied $(A_{14-x}A'_x)Cu_{24}O_{41}$ ($A$ = alkaline-earth metal, $A'$ = trivalent metal). All of these studies showed that there are two sets of orthorhombic sublattices in the crystals with periods $c_1 \simeq 0{\cdot}390$ and $c_2 \simeq 0{\cdot}275$ nm. It was recognized that the sublattice with $c_1 \simeq 0{\cdot}390$ nm is related to a sheet of $Cu_2O_3$ with the Sr and Ca atoms, while the sublattice with $c_2 \simeq 0{\cdot}275$ nm is composed of a $CuO_2$ chain. The structures of the crystals have been determined by Kato *et al.* (1988) using a superlattice $c = 5 \times 0{\cdot}390 \simeq 7 \times 0{\cdot}275$ nm and by McCarron *et al.* (1988) and Siegrist *et al.* (1988) using a larger superlattice, $c = 7 \times 0{\cdot}390 \simeq 10 \times 0{\cdot}275$ nm.

In the present work, a transmission electron microscope (TEM) is used to study the crystal structure of $(Sr_{1.5}Ca_{1.5})Cu_{5+\delta}O_y$. The diffraction streaks in the electron diffraction patterns (EDPs) are studied in detail and some high-resolution electron-microscope images are shown.

## 2. Experimental

The sample was prepared by a solid-state reaction. Starting reagents, $CaCO_3$, $SrCO_3$ and CuO, were mixed mechanically in the ratio Ca:Sr:Cu = 1·5:1·5:5, shaped into a pellet and fired at 1123 K in air for 5 d with intermediate grinding.

Two different methods were used to prepare thin specimens for TEM observation. The first one was to grind the sample pellet in an agate mortar. The small crystal fragments obtained were mounted on a microgrid. In this case the crystal fragments were often arrayed with the (100) plane parallel to the microgrid plane. In the other case the sample pellet was polished mechanically down to a thickness of less than 50 μm and then thinned in a Gatan 600N-DP ion-milling machine at an accelerating voltage of 6 kV.

A JEM-2000EX TEM operated at an accelerating voltage of 200 kV was used to observe the specimens.

## 3. Electron diffraction patterns (EDPs)

Figs. 1(*a*), (*b*), (*c*) and (*d*) are EDPs taken along the [001], [010], [100] and [1$\bar{1}$0] directions, respectively. From (*b*), (*c*) and (*d*) we find that there is an incommensurate modulation structure along the $c^*$ axis. There are some extra weak diffraction spots along the $c^*$ axis in (*d*). The appearance of these extra spots is rather difficult to explain by either a displacive or a compositional modulation model. We introduce two sets of independent orthorhombic sublattices $L_1$ and $L_2$ to describe this crystal. The sublattice parameters are $a = a_1 = a_2 = 1{\cdot}28$, $b = b_1 = b_2 = 1{\cdot}13$, $c_1 = 0{\cdot}390$

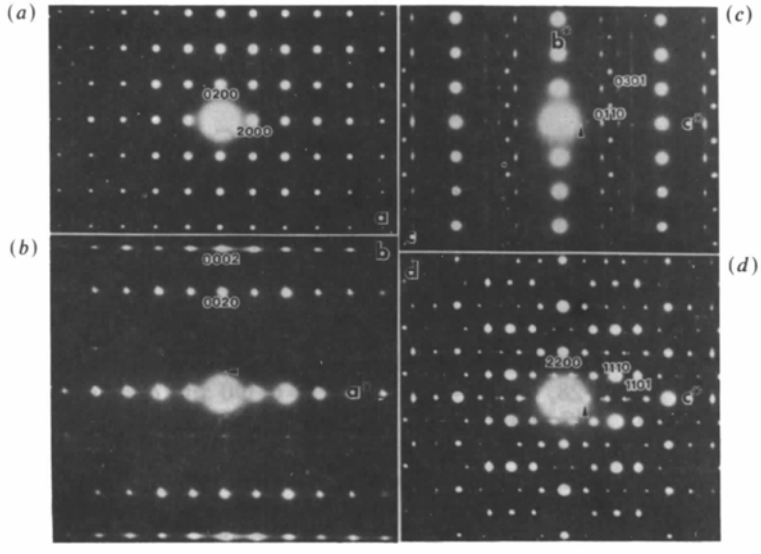


Fig. 1. EDPs taken from an $(Sr_{1.5}Ca_{1.5})Cu_{5+\delta}O_y$ crystal along (*a*) [001], (*b*) [010], (*c*) [100] and (*d*) [1$\bar{1}$0] directions. Using four indices $hkl_1l_2$ we can index all of the diffraction spots. The streaks passing through $hkl_1l_2$ ($l_2 \neq 0$) are visible in (*b*), (*c*) and (*d*).

and $c_2 = 0{\cdot}275$ nm, respectively. In the EDPs, the third index is related to $L_1$ and the fourth one is related to $L_2$. From the standpoint of kinematical diffraction we get the diffraction pattern of the $[1\bar{1}0]$ projection like Fig. 2(*a*); the gray spots are from $L_1$ and the small full circles are from $L_2$. Large full circles are common to both sublattices. We then consider dynamical diffraction. Since the intensity of spots from $L_1$ is much stronger than that from $L_2$, the gray spots must act as the source of double diffraction. In Fig. 2(*b*) open circles indicate the double diffraction spots while the crosses indicate the triple diffraction ones. Evidently, Fig. 2(*b*) is in agreement with Fig. 1(*d*). That there are two sets of sublattice in a crystal means that the crystal has a chimney ladder structure (Ye & Amelinckx, 1986). Using four indexes $(hkl_1l_2)$ we can index all the EDPs in Fig. 1.

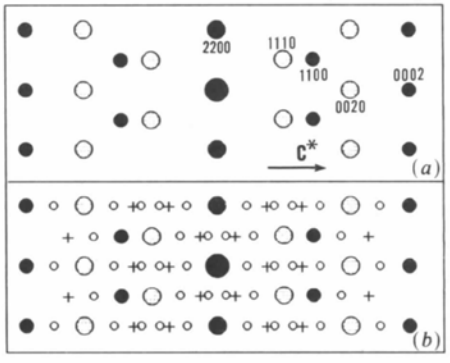


Fig. 2. A chimney ladder structure gives a diffraction pattern (*a*) under the assumption of kinematical diffraction. Under multiple diffraction, on the other hand, (*b*) is obtained. The electron beam is incident along $[1\bar{1}0]$ of $(Sr_{1\cdot5}Ca_{1\cdot5})Cu_{5+\delta}O_y$. Small open circles indicate double diffraction and crosses indicate triple diffraction. (*b*) is similar to Fig. 1(*d*).

The diffraction spots for both of the sublattices satisfy the extinction rule of space group *Fmmm* (or *F*222 or *Fmm*2) in every EDP, except for Fig. 1(*c*) which is taken along [100], in which the forbidden spots 0110, 0101 *etc.* appear. Since the extra spots are much weaker than the normal spots, they do not seem to be fundamental ones and must have been produced by the imperfection of the crystal. One reasonable explanation for spots 0110 *etc.* from $L_1$ is that the distribution of Sr and Ca atoms is partly ordered. This will be confirmed by the following observation.

Figs. 3(*a*) and (*b*) show the EDPs taken along [100] from the specimens which have been prepared by crushing and by an ion-milling method, respectively. The extra spots along the arrows in (*a*) come from $L_1$. They do not arise in (*b*). This means that there is a structure change in the $L_1$ lattice during ion milling. On the other hand, the extra spots related to $L_2$ remain in (*b*). This means that the origins of the anomalous spots from $L_1$ and $L_2$ are different. In fact, diffraction streaks always pass through the spots from $L_2$. The occurrence of these streaks implies that the structure of $L_2$ is disordered. Accordingly, we propose that the extra spots of $L_2$ are related to this disordered structure, which will be discussed in the next section.

We may conclude according to the results of EDP analysis that the structure of the present crystal $(Sr_{1\cdot5}Ca_{1\cdot5})Cu_{5+\delta}O_y$ is similar to that of $M_{10}Cu_{17}O_{29}$ and $(Sr_{14-x}Ca_x)Cu_{24}O_{41}$. In order to calculate the diffraction intensity and the simulation image we have to use a superlattice model with $c = 5 \times 0{\cdot}290 \simeq 7 \times 0{\cdot}275$ nm, as has been proposed by Kato *et al.* (1988), in which the atom coordinates for each sublattice were determined by McCarron *et al.* (1988). Using this model, it is not necessary to use the fourth index as we did in Figs. 1 and 2; for example, the spot 0020 in Figs. 1(*b*), (*c*) and (*d*) should then be labeled

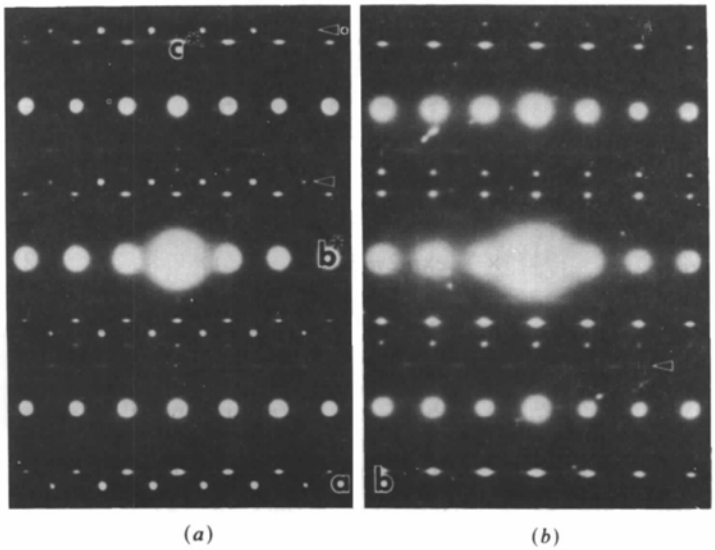


(*a*) (*b*)

Fig. 3. EDPs taken along $[1\bar{1}0]$ from (*a*) a specimen prepared by crushing and (*b*) a specimen prepared by ion milling. The extra spots related to $L_1$ appear in (*a*) as indicated by arrows but disappear in (*b*). Those related to $L_2$ still remain after ion irradiation as indicated by the arrow in (*b*).

0,0,10 and the weaker spot nearest to the center spot in Fig. 1(*d*) as 002.

Fig. 4 shows the ratio of the calculated amplitude of the 002 diffraction spot to that of 0,0,10 as a function of crystal thickness. The ratios have a strong dependence on the incident direction of the electron beam. In the cases of [100] and [010] incidence, the ratios are always around 0·1%, while in the case of $[1\bar{1}0]$ incidence the ratios increase from 1 to 7%. According to the calculation, the intensity of the 002 spot from $[1\bar{1}0]$ incidence should be much stronger than that from [100] or [010] incidence. Indeed, the 002 spot, which is the weak one near the center spot indicated by an arrow in Fig. 1(*d*), can be seen clearly, while there is no spot at the corresponding position indicated by the arrow in (*b*) and (*c*). The calculation is in good agreement with observation. We may say that the superlattice model used here is a good approximation for describing the crystal structure.

## 4. Diffraction streaks due to the initial phase disorder of the $L_2$ sublattice

In Figs. 1(*b*), (*c*) and (*d*) we have found that there are always some streaks normal to the $c^*$ direction, which pass through only the spots $(hkl_1l_2)$ $(l_2 \neq 0)$. Evidently, there is a group of planes parallel to the $\mathbf{a}^*\mathbf{b}^*$ plane in reciprocal space.

Very similar diffraction patterns have been observed in some hollandite-type crystals (Cadee & Prodan, 1979; Suzuki, Tanaka, Ishigame, Suemoto, Shibata, Onoda & Fujiki, 1986; Zandbergen, Everstijn, Mijlhoff, Renes & Ijdo, 1987; Wu, Li & Hashimoto, 1990). It has been proved that the crystal has a displacive modulation structure and the initial phase disorder (IPD) of the modulation waves produces these streaks (Wu & Horiuchi, 1991; Wu, Fujiki, Ishigame & Horiuchi, 1991).

The modulation mechanism of $(Sr_{1\cdot5}Ca_{1\cdot5})Cu_{5+\delta}O_y$ is different from the hollandite-type crystals but the resemblance of the diffraction patterns suggests that the $(Sr_{1\cdot5}Ca_{1\cdot5})Cu_{5+\delta}O_y$ crystal may also have a structure with initial phase disorder. In this case an initial phase disorder means that the origin of the sublattice $L_2$ is disordered, *i.e.* there is no constant vector of three-dimensional translation for $L_2$ in real space.

In the crystal of $(Sr_{1\cdot5}Ca_{1\cdot5})Cu_{5+\delta}O_y$ the sheets of $Cu_2O_3$ together with Sr and Ca atoms form a sublattice $L_1$, while the $CuO_2$ chains form another sublattice $L_2$, which is incommensurate to $L_1$ along the $c$ axis. In other words, if the origin of $L_1$ is fixed, the $z$ coordinate of the origin of $L_2$ is always changed. That is to say, we can select the origin $z$ coordinate of $L_2$ arbitrarily without any change for describing the fundamental crystal structure. This implies physically that the interaction between these two sublattices is very weak. On the other hand, every $CuO_2$ chain independently completes the chemical bond so that the interaction between adjoining chains must be weak. In local areas the $CuO_2$ chains start with the same phase, while in other areas the $CuO_2$ chains possibly start with different phases.

In the case of a displacive modulation structure, it has been proved that an IPD model can produce streaks in EDPs. Now the question is whether an IPD model with the chimney ladder structure produces such streaks.

In the chimney ladder structure any atom can be classified in any of the sublattices. In a simple case, we assume that there are only two sublattices $L_1$ and $L_2$ with different periods $c_1$ and $c_2$. As a first step, we consider a crystal with two sets of perfect sublattices. Let us denote the $j$th-atom position in $L_1$ by $\mathbf{r}_j = x_j\mathbf{a} + y_j\mathbf{b} + z_j\mathbf{c}_1$ and by $\mathbf{r}'_j = x'_j\mathbf{a} + y'_j\mathbf{b} + z'_j\mathbf{c}_2$ in $L_2$. $\mathbf{c}_1 = q\mathbf{c}_2$ in real space and $\mathbf{c}_2^* = q\mathbf{c}_1^*$ in reciprocal space, where $q$ is irrational. In the following discussion all parameters with a prime are related to $L_2$.

The structure factor $F(uvw)$ can be expressed as

$$F(uvw) = \sum_j f_j \exp 2\pi i\mathbf{H}\cdot\mathbf{r}_j + \sum_j f'_j \exp 2\pi i\mathbf{H}\cdot\mathbf{r}'_j \quad (1)$$

where $f_j$ means the atomic scattering factor of the $j$th atom in $L_1$, $f'_j$ the atomic scattering factor of the $j$th atom in $L_2$, $\mathbf{H} = u\mathbf{a}^* + v\mathbf{b}^* + w\mathbf{c}_1^*$ the vector in reciprocal space, $u$, $v$ and $w$ are real numbers.

The number of unit cells along the directions $a$, $b$ and $c$ are $N_1$, $N_2$ and $N_3$ for $L_1$ and $N'_1$, $N'_2$ and $N'_3$ for $L_2$ respectively. We take $N = N_1N_2N_3$ and $N' = N'_1N'_2N'_3$. The diffraction intensity at the position $(uvw)$ should be written as

$$\begin{aligned} I(uvw) &\propto \left| \sum_{\mathbf{n},\mathbf{n}'}^{N,N'} F(uvw) \right|^2 \\ &= (1/N)^2 \sum_{i,j} f_i f_j \exp 2\pi i\mathbf{H}\cdot(\mathbf{r}_i - \mathbf{r}_j) \\ &\quad \times \sum_{\mathbf{n},\mathbf{m}} \exp 2\pi i\mathbf{H}\cdot(\mathbf{R}_\mathbf{n} - \mathbf{R}_\mathbf{m}) \\ &\quad + (1/N')^2 \sum_{i,j} f'_i f'_j \exp 2\pi i\mathbf{H}\cdot(\mathbf{r}'_i - \mathbf{r}'_j) \\ &\quad \times \sum_{\mathbf{n}',\mathbf{m}'} \exp 2\pi i\mathbf{H}\cdot(\mathbf{R}_{\mathbf{n}'} - \mathbf{R}_{\mathbf{m}'}) \\ &\quad + (1/NN')2\,\mathrm{Re}\left\{ \sum_{i,j} f_i f'_j \exp 2\pi i\mathbf{H}\cdot(\mathbf{r}_i - \mathbf{r}'_j) \right. \\ &\quad \left. \times \sum_{\mathbf{n},\mathbf{n}'} \exp 2\pi i\mathbf{H}\cdot(\mathbf{R}_\mathbf{n} - \mathbf{R}_{\mathbf{n}'}) \right\} \end{aligned} \quad (2)$$

where $\mathbf{R}_\mathbf{n} = n_1\mathbf{a} + n_2\mathbf{b} + n_3\mathbf{c}_1$ and $\mathbf{R}_{\mathbf{n}'} = n'_1\mathbf{a} + n'_2\mathbf{b} + n'_3\mathbf{c}_2 = n'_1\mathbf{a} + n'_2\mathbf{b} + n'_3\mathbf{c}_1/q$ are translation vectors for $L_1$ and $L_2$, respectively. $\mathbf{n} = (n_1, n_2, n_3)$ and $\mathbf{n}' = (n'_1, n'_2, n'_3)$ with $n_1$, $n_2$, $n_3$, $n'_1$, $n'_2$ and $n'_3$ integers. Re means the real part of the bracket. The right part of the equation consists of three terms; the first one is from $L_1$, the second one from $L_2$ and the third one from both of the sublattices. For each term, the

contribution from the first summation gives a constant phase factor, which can be written as $C_1$, $C_2$ and $C_3$, respectively.

Substituting **H** and **R**, we have for each term

$$\begin{aligned} T_1 &= (C_1/N^2)\sum_{\mathbf{n},\mathbf{m}} \exp 2\pi i[u(n_1-m_1) \\ &\quad +v(n_2-m_2)+w(n_3-m_3)] \\ &= (C_1/N^2)\sum_{n_1,m_1}\exp 2\pi iu(n_1-m_1) \\ &\quad \times \sum_{n_2,m_2}\exp 2\pi iv(n_2-m_2) \\ &\quad \times \sum_{n_3,m_3}\exp 2\pi iw(n_3-m_3) \\ &= C_1\delta_{uh}\delta_{vk}\delta_{wl} \end{aligned} \tag{3}$$

$$\begin{aligned} T_2 &= (C_2/N'^2)\sum_{\mathbf{n}',\mathbf{m}'} \exp 2\pi i[u(n_1'-m_1') \\ &\quad +v(n_2'-m_2')+w(n_3'-m_3')/q] \\ &= (C_2/N'^2)\sum_{n_1',m_1'}\exp 2\pi iu(n_1'-m_1') \\ &\quad \times \sum_{n_2',m_2'}\exp 2\pi iv(n_2'-m_2') \\ &\quad \times \sum_{n_3',m_3'}\exp 2\pi iw(n_3'-m_3')/q \\ &= C_2\delta_{uh}\delta_{vk}\delta_{w(ql)} \end{aligned} \tag{4}$$

$$\begin{aligned} T_3 &= 2\,\mathrm{Re}\left\{(C_3/N'N)\sum_{\mathbf{n},\mathbf{n}'}\exp 2\pi i[u(n_1-n_1') \right. \\ &\quad \left. +v(n_2-n_2')+w(n_3-n_3'/q)]\right\} \\ &= 2\,\mathrm{Re}\left\{(C_3/N'N)\sum_{n_1,n_1'}\exp 2\pi iu(n_1-n_1') \right. \\ &\quad \times \sum_{n_2,n_2'}\exp 2\pi iv(n_2-n_2') \\ &\quad \left. \times \sum_{n_3,n_3'}\exp 2\pi iw(n_3-n_3'/q)\right\} \\ &= 2\,\mathrm{Re}\,[C_3]\delta_{uh}\delta_{vk}\delta_{w0} \end{aligned} \tag{5}$$

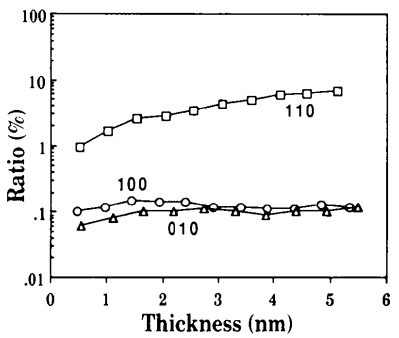


Fig. 4. Ratio of the calculated amplitude of the 002 diffraction spot to that of 0,0,10 as a function of the thickness for different incident orientations [100], [010] and [1$\bar{1}$0]. A superlattice with $c = 1{\cdot}95$ nm is used for the calculation.

where $h$, $k$, $l$ are integers and $\delta$ is a delta function. Accordingly, the diffraction intensity is directly proportional to

$$\begin{aligned} T_1+T_2+T_3 &= C_1\delta_{uh}\delta_{vk}\delta_{wl}+C_2\delta_{uh}\delta_{vk}\delta_{w(ql)} \\ &\quad +2\,\mathrm{Re}\,[C_3]\delta_{uh}\delta_{vk}\delta_{w0}. \end{aligned} \tag{6}$$

From this formula we know that there are two kinds of diffraction spots in reciprocal space. The first is related to $T_1$ and $T_3$ with indexes $hkl$, while the second is related to $T_2$ with indexes $h,k,ql$. The last index $ql$ of $T_2$ is irrational. If we introduce a new basic vector $\mathbf{c}_2^* = q\mathbf{c}_1^* = q\mathbf{c}^*$, every lattice point in reciprocal space can be expressed as $hkl_1l_2$. It is also known from (6) that we can get diffraction spots $hkl_10$ ($l_1 \neq 0$) from $L_1$, $hk0l_2$ ($l_2 \neq 0$) from $L_2$ and $hk00$ from both $L_1$ and $L_2$, while diffraction spots like $hkl_1l_2$ ($l_1, l_2 \neq 0$) do not appear unless any multiple diffraction is excited. This means that under the condition of kinematical approximation, which is usually satisfied by X-ray diffraction (Jensen, Larsen, Maly & Coppens, 1990), the atom positions in sublattice $L_1$ (or $L_2$) can be determined from diffraction spots $hkl_10$ ($l_1 \neq 0$) [or $hk0l_2$ ($l_2 \neq 0$)] and the $x$ and $y$ coordinates of the origin of $L_2$ relative to $L_1$ can be determined from the spots $hk00$. Owing to the incommensuration between $L_1$ and $L_2$ along the $c$ axis it is meaningless to discuss the relative $z$ coordinate.

When the initial phase along the $c$ direction is disordered in the sublattice $L_2$, the structure of reciprocal space becomes variable. In this case the translation vector $\mathbf{R}_{\mathbf{n}'}$ is no longer constant but is written as

$$\begin{aligned} \mathbf{R}_{\mathbf{n}'} &= n_1'\mathbf{a}+n_2'\mathbf{b}+[n_3'+\Delta(n_1', n_2')]\mathbf{c}_2 \\ &= n_1'\mathbf{a}+n_2'\mathbf{b}+[n_3'+\Delta(n_1', n_2')]\mathbf{c}_1/q, \end{aligned} \tag{7}$$

where $\Delta(n_1', n_2')$ is a random function between 0 and 1.

By substitution of (7) into (4), $T_2$ becomes

$$\begin{aligned} T_2 &= (C_2/N'^2)\sum_{\mathbf{n}',\mathbf{m}'}\exp 2\pi i\{u(n_1'-m_1')+v(n_2'-m_2') \\ &\quad +w(n_3'-m_3')/q+w[\Delta(n_1', n_2')-\Delta(m_1', m_2')]/q\} \\ &= (C_2/N'^2)\sum_{n_1',m_1',n_2',m_2'}\exp 2\pi i\{u(n_1'-m_1') \\ &\quad +v(n_2'-m_2')+w[\Delta(n_1', n_2')-\Delta(m_1', m_2')]/q\} \\ &\quad \times \sum_{n_3',m_3'}\exp 2\pi iw(n_3'-m_3')/q \\ &= C_2/(N_1N_2)^2\delta_{w(ql)} \\ &\quad \times \sum_{n_1',m_1',n_2',m_2'}\exp 2\pi i\{u(n_1'-m_1')+v(n_2'-m_2') \\ &\quad +w[\Delta(n_1', n_2')-\Delta(m_1', m_2')]/q\}. \end{aligned} \tag{8}$$

Clearly, after introducing $\Delta$, the summation on $n_1'$ and $n_2'$ no longer leads to a $\delta$ function. There is no limitation for indices $u$ and $v$. Along the direction

$c^*$, on the other hand, $T_2$ is non-zero only when $w = ql$. This means that there is a set of reflection planes in reciprocal space which is parallel to $a^*b^*$ and are separated from each other with spacing $nqc_1^* = nc_2^*$ ($n$ = integer). When $w = 0$ (9) becomes (4) and only sharp diffraction spots $hk00$ appear.

Substituting (7) into (5), we have

$$T_3 = 2\,\mathrm{Re}\left\{[C_3\delta_{w0}/(N_1N_2)^2] \times \sum_{n',m'} \exp 2\pi i[u(n_1'-m_1')+v(n_2'-m_2') - w\Delta(m_1', m_2')/q]\right\}. \quad (9)$$

Similar to (8) the whole formula becomes (5) when $w = 0$. When $w \neq 0$, however, $T_3$ becomes zero owing to the effect of the $\delta$ function. In other words, the contribution of $T_3$ remains unchanged after changing $\mathbf{R}_{n'}$.

We can conclude that when the initial phase of $L_2$ is disordered the change in reciprocal space is expressed only by $T_2$; diffraction spots $hkl_10$ are always sharp, while the reflection planes $(uv0l_2)$ $(l_2 \neq 0)$ appear instead of sharp spots $hk0l_2$.

The discussion here is based on the assumption that all the $L_2$ sublattices are completely disordered, namely, $\Delta(n_1', n_2')$ always changes. In this case, $T_2$ gives only diffraction planes but no spots at all when $l_2 \neq 0$.

However, the result will be changed if the initial phase of $L_2$ is partially disordered, *i.e.* some of the $L_2$ sublattice rows start with the same phase while others are disordered. In this case, $T_2$ should be separated into two parts. One part is related to the ordered sublattice rows, which causes sharp diffraction spots $hk0l_2$, while another part is related to the rows with the initial phase disorder, which causes a set of reflection planes $(uv0l_2)$ $(l_2 \neq 0)$. Diffraction spots $hk0l_2$ always locate on the reflection planes $(uv0l_2)$.

These discussions can be examined easily by means of optical diffraction. Fig. 5($a$) shows a perfect two-dimensional chimney ladder structure with $b_1/b_2 = 2^{1/2}$. Fig. 5($b$) is an optical diffraction pattern (ODP) corresponding to ($a$). We can find two sets of independent spots $hk_10$ and $h0k_2$. Since no multiple

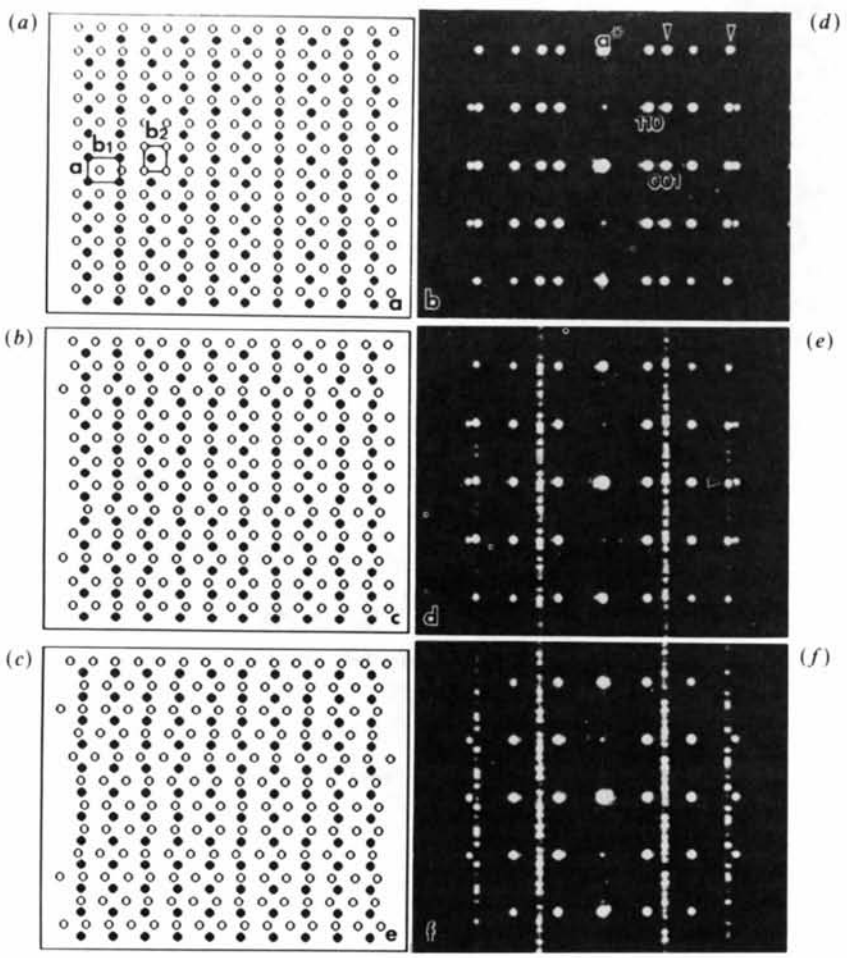


Fig. 5. ($a$) A two-dimensional model for a perfect chimney ladder structure with $b_1/b_2 = 2^{1/2}$. ($b$) An ODP corresponding to ($a$). Since no multiple diffraction occurs, there are no spots $hk_1k_2$ $(k_1, k_2 \neq 0)$. ($c$) A model with the initial phase disorder in about one third of $L_2$. ($d$) An ODP corresponding to ($c$). An arrow is drawn to indicate the spot from $L_2$. Not only spots but also streaks are seen along the line $(u0k_2)$ $(k_2 \neq 0)$. ($e$) A model with complete initial phase disorder in $L_2$. ($f$) An ODP corresponding to ($e$). No spots but streaks are seen along the line $(u0k_2)$ $(k_2 \neq 0)$. The variation from ($b$) to ($f$) can be seen clearly along the direction indicated by the arrows in ($b$).

diffraction occurs, there are no $hk_1k_2$ ($k_1$, $k_2 \neq 0$) spots at all. When an initial partial phase disorder is introduced in Fig. 5(*c*), where one third of the rows start with different $z$ coordinates, the streaks ($u0k_2$) ($k_2 \neq 0$) appear in the corresponding ODP (*d*) together with the diffraction spots $h0k_2$. When the initial phase is disordered completely as shown in Fig. 5(*e*), only streaks ($u0k_2$) occur without any spots in the corresponding ODP (*f*). The ODPs are in good agreement with the mathematical inference as well as the EDPs. Comparing Figs. 1 and 5 we can conclude that in the $(Sr_{1.5}Ca_{1.5})Cu_{5+\delta}O_y$ crystal the initial phase of $CuO_2$ chains is partially disordered.

## 5. Observed and calculated high-resolution images

Fig. 6(*a*) is a projection of the crystal structure along the [001] direction. The bold line indicates the unit cell of $L_2$, while the dashed line indicates the unit cell of $L_1$. The shift of the origin in $L_2$ relative to that in $L_1$ is $x = 0{\cdot}75$ and $y = 0{\cdot}75$ as proposed by McCarron *et al.* (1988). Fig. 6(*b*) is a projection of the crystal lattice along the *a* axis. The full dots indicate the sublattice points of $L_1$ and the open circles the sublattice points of $L_2$. Owing to incommensuration between $L_1$ and $L_2$ no superperiod exists.

Figs. 7(*a*) and (*b*) are the high-resolution images taken along [001] together with the corresponding simulation images. In order to calculate the images, a superlattice with $c = 1{\cdot}95$ nm, *i.e.* $c = 5 \times c_1 \sim 7 \times c_2$, is used. In (*a*) a projection of the structure along [001] is inserted. The calculations show that image (*a*) is taken with a thickness of 1·95 nm at an underfocus of 50 nm and image (*b*) is with a thickness of 4·87 nm at 35 nm underfocus. In (*a*) the white dots correspond to the positions of Sr or Ca and Cu atoms. The observed and calculated images are in good agreement.

There is, however, no information about the modulation structure from the images taken along the [001] direction. The modulation structure can be observed when the electron beam is incident normal to the *c* axis. According to the calculation shown in Fig. 4, where the electron beam is incident along [1$\bar{1}$0], the weak spots related to the modulation structure are much stronger than that from the [100] or [010] incidence. This means that the [1$\bar{1}$0] incidence is the best orientation to observe the modulation structure.

Fig. 8(*a*) is a TEM image taken along [1$\bar{1}$0], which shows the modulation fringes clearly. The spacing between adjoining fringes, marked by large arrows in an enlarged image (*b*), is equal to $1/|\mathbf{c}_1^* - \mathbf{c}_2^*|$, which is incommensurate with either $\mathbf{c}_1$ or $\mathbf{c}_2$. The spacing of the modulation is not an integral multiple of the subspacing indicated by the smaller arrows. Even if we use a longer period, which is obtained as an integral multiple of the modulation spacing, there is no integer relationship between the modulation spacing and the subspacing. It should be noticed that the fringes in Fig. 8(*a*) are not on a straight line, but shift prominently from the right to the left. At a constant defocus there are two possible factors to make the fringe shift. One is a change in crystal thickness and the other is a change in atom positions.

Using the superlattice mentioned above, a series of simulated images along [1$\bar{1}$0] are calculated with an underfocus of 25 nm as the thickness increases (Fig. 9). The thickness of Fig. 9(*a*) is 3·4, (*b*) 4·3,

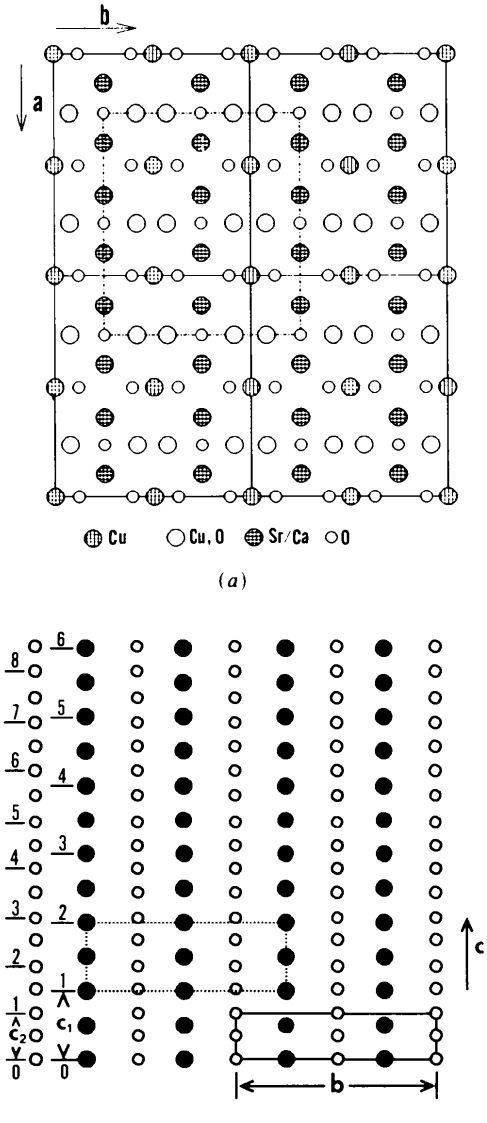


Fig. 6. (*a*) The projection of atoms in an $(Sr_{1.5}Ca_{1.5})Cu_{5+\delta}O_y$ crystal along [001]. The dashed line shows the sublattice $L_1$ and the solid line the sublattice $L_2$. (*b*) The projection of the crystal lattice along the *a* axis. The filled and open circles indicate the sublattice points of $L_1$ and $L_2$, respectively. The dashed line shows the unit cell of $L_1$ and the solid line that of $L_2$. Both sublattices simultaneously start at level 0 as shown in the figure. They do not coincide with each other at all along the *c* direction.

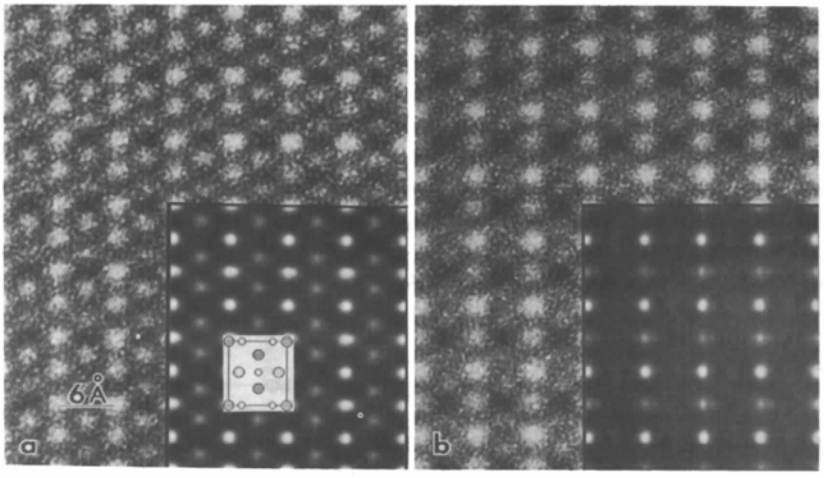


(*a*) (*b*)

Fig. 7. The high-resolution images taken along (*a*) [001] with a thickness of about 2 nm at underfocus of 50 nm and (*b*) with a thickness of about 5 nm at underfocus of 35 nm. The corresponding simulated images are inserted in (*a*) and (*b*) and a structure projection is also inserted in (*a*).

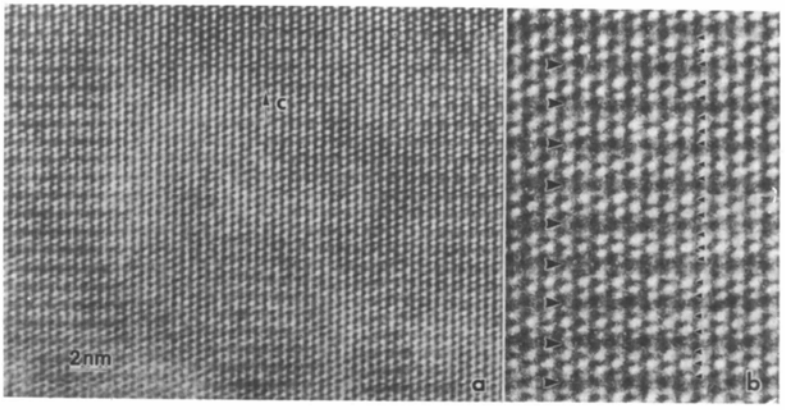


(*a*) (*b*)

Fig. 8. (*a*) High-resolution image taken along [1$\bar{1}$0] and (*b*) an enlargement from part of (*a*). The modulation fringes shift from the right part to the left part in (*a*). In (*b*) the larger arrows indicate the modulation spacing while the smaller arrows indicate the subspacing.

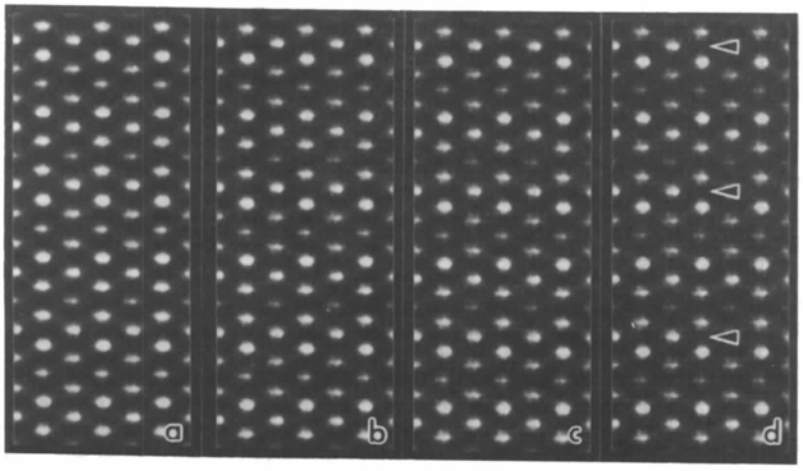


(*a*) (*b*) (*c*) (*d*)

Fig. 9. A series of high-resolution images simulated at the underfocus of 25 nm with thickness (*a*) 3·4, (*b*) 4·3, (*c*) 5·1 and (*d*) 6·0 nm along [1$\bar{1}$0]. The arrows indicate the modulation fringes. Obviously, there is no fringe shift as the thickness increases.

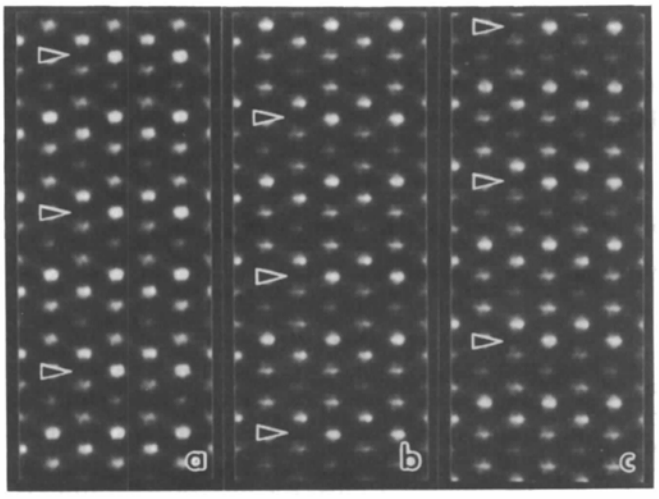


(*a*) (*b*) (*c*)

Fig. 10. A series of high-resolution images simulated along [1$\bar{1}$0] at an underfocus of 25 nm with a thickness of 5·1 nm. The origin of $L_2$ is changed relative to that of $L_1$ with a step of 0·585 Å from (*a*) to (*c*) along the *c* direction. The fringe shift indicated by arrows is very large in spite of the small translation of the origin.

(*c*) 5·1 and (*d*) 6·0 nm. Though the image does not match the observed ones very well mainly due to the assumption of a commensurate superlattice, the modulation fringes can be seen clearly along the direction indicated by the arrows. As a result we notice that thickness variation causes almost no fringe shift in the images.

When the *z* coordinates of $CuO_2$ chains ($L_2$ sublattice) are changed relative to the $Cu_2O_3$ sheet ($L_1$ sublattice), we get the simulation images in Fig. 10 for the thickness of 5·1 nm at the underfocus of 25 nm. Though the translation of the origin of $CuO_2$ chains is very slight (less than 0·6 Å) along the **c** direction, the fringe shift is very marked.

Comparing Figs. 8 and 10, we can conclude that the fringe shift is due to the translation of the origin of $CuO_2$ chains. That is to say, the $CuO_2$ chains start with different *z* coordinate from area to area. In other words, the initial phase of the sublattice $L_2$ is partially disordered. This result together with the diffraction analysis in the preceding section gives strong support to the structure model with IPD.

## 6. Summary

The analysis on EDPs shows that there are two sets of sublattices in a crystal $(Sr_{1\cdot5}Ca_{1\cdot5})Cu_{5+\delta}O_y$, which are incommensurate along the *c* axis with parameters $c_1 = 0\cdot390$ and $c_2 = 0\cdot275$ nm. The sublattice $L_1$ is composed of $Cu_2O_3$ sheets parallel to **bc** and $L_2$ is composed of $CuO_2$ chains along the *c* axis. In EDPs there are some streaks always passing through the spots related to $L_2$. This means that there is a set of reflection planes in reciprocal space. These planes come from the partial disorder in the initial phase of $L_2$. It has been proved by a mathematical inference as well as an optical diffraction method that the initial phase disorder (IPD) model in the chimney ladder structure can cause such a set of reflection planes in reciprocal space. As more evidence for the IPD model we have observed the shift of modulation fringes in high-resolution TEM images.

The authors express their sincere gratitude to Dr K. Kato for his valuable suggestions, Dr Y. Matsui for the computer calculations and Messrs Y. Kitami and M. Yokoyama for the EM maintenance. One of the authors (XJW) expresses his sincere appreciation to the Science and Technology Agency, Japan, for offering the fellowship.

### References

CADEE, M. C. & PRODAN, A. (1979). *Mater. Res. Bull.* **14**, 613–618.
HORIUCHI, S., SHODA, K., WU, X. J., NOZAKI, H. & TSUTSUMI, M. (1990). *Physica (Utrecht)*, C**168**, 205–214.
JENSEN, A. F., LARSEN, F. K., MALY, K. & COPPENS, P. (1990). *Acta Cryst.* A**46**, C395–C396.
KATO, K., TAKAYAMA-MUROMACHI, E., KOSUDA, K. & UCHIDA, Y. (1988). *Acta Cryst.* C**44**, 1881–1884.
MCCARRON, E. M., SUBRAMANIAN, M. A., CALABRESE, J. C. & HARLOW, R. L. (1988). *Mater. Res. Bull.* **23**, 1355–1365.
SIEGRIST, T., SCHNEEMEYER, L. F., SUNSHINE, S. A., WASZCZAK, J. V. & ROTH, R. S. (1988). *Mater. Res. Bull.* **23**, 1429–1438.
SUZUKI, S., TANAKA, M., ISHIGAME, M., SUEMOTO, T., SHIBATA, Y., ONODA, Y. & FUJIKI, Y. (1986). Proc. XI Int. Congr. on Electron Microscopy, Kyoto, Japan, pp. 1717–1718.
WU, X. J., FUJIKI, Y., ISHIGAME, M. & HORIUCHI, S. (1991). *Acta Cryst.* A**47**, 404–413.
WU, X. J. & HORIUCHI, S. (1991). *Acta Cryst.* A**47**, 11–16.
WU, X. J., LI, F. H. & HASHIMOTO, H. (1990). *Acta Cryst.* B**46**, 111–117.
YE, H. Q. & AMELINCKX, S. (1986). *J. Solid State Chem.* **61**, 8–39.
ZANDBERGEN, H. W., EVERSTIJN, P. L. A., MIJLHOFF, F. C., RENES, G. H. & IJDO, D. J. W. (1987). *Mater. Res. Bull.* **22**, 431–438.